AJNR

# The Cerebellum in Sagittal Plane—Anatomic-MR Correlation: 1. The Vermis

Eric Courchesne, Gary A. Press, James Murakami, Dean Berthoty, Marjorie Grafe, Clayton A. Wiley and John R. Hesselink

*AJNR Am J Neuroradiol* 1989, 10 (4) 659-665
http://www.ajnr.org/content/10/4/659

# The Cerebellum in Sagittal Plane—Anatomic-MR Correlation: 1. The Vermis

Eric Courchesne[1]
Gary A. Press[2]
James Murakami[1]
Dean Berthoty[2]
Marjorie Grafe[3]
Clayton A. Wiley[3]
John R. Hesselink[2]

**Correlation of thin (5-mm) sagittal high-field (1.5-T) MR images of three brain specimens and 11 normal volunteers with microtome sections of the human cerebellar vermis and hemispheres demonstrates that proton-density-weighted (long TR/short TE) and T2-weighted (long TR/long TE) spin-echo pulse sequences provide the greatest contrast between gray and white matter. These images also can display (1) the corpus medullare and primary white-matter branches to the vermian lobules, including the lingula, centralis, culmen, declive, folium, tuber, pyramis, uvula, and nodulus; and (2) several finer secondary branches to individual folia within the lobules. Surface features of the vermis including the deeper fissures (e.g., preculminate, primary, horizontal, and prepyramidal) and shallower sulci are best delineated by T1-weighted (short TR/short TE) and T2-weighted images, which provide greatest contrast between CSF and parenchyma. Given that the width of the normal vermis varied from 6 to 12 mm in our volunteers, the acquisition of thin slices (≤5 mm) was required to minimize volume averaging of the cerebellar hemispheres with the vermis on a midline sagittal MR section.**

**Knowledge of the detailed normal anatomy of the cerebellar vermis on sagittal MR images can assist in the identification of various pathologic alterations.**

Previous reports provided initial descriptions of normal and pathologic anatomy of the posterior fossa contents at low [1–3], moderate [4, 5], and high [6–9] MR field strengths. Compared with high-resolution CT, MR imaging demonstrates more detailed anatomy of the brainstem, cerebellopontine angles, and internal auditory canals due to its multiplanar imaging capability, absence of beam-hardening artifacts, and greater intrinsic soft-tissue contrast [9].

Although descriptions of the MR appearance of congenital and acquired abnormalities of the cerebellum are included in several reports [2, 4, 10–15], improvements in MR technology including thin (3- to 5-mm) sections, special flow-compensating spin-echo pulse sequences, and cardiac gating now permit display of normal anatomic features of the cerebellum not shown previously. Thus, it seems useful to determine the MR resolution of the cerebellar lobes, lobules, fissures, and related posterior fossa structures by correlating MR with myelin-stained sections of the human cerebellum. Application of these normative data to cerebellar abnormalities, particularly congenital malformations, will be the subject of a separate report.

## Materials, Subjects, and Methods

MR studies of three formalin-fixed cadaver brains and 11 normal, healthy adult volunteers, 10 males and one female 13–38 years old (mean age, 24.5 years), were performed in three orthogonal planes by using a 1.5-T superconducting magnet.* All volunteers and specimens were imaged with a standard head coil. In all instances, 5-mm slices with a field of view (FOV) of 12–18 cm and matrix size of 256 × 256 were acquired using spin-echo sequences. T1-weighted sequences had the parameters, 600/20/4–6 (TR/TE/excitations). All volunteers

* General Electric, Milwaukee, WI.

**This article appears in the July/August 1989 issue of *AJNR* and the October 1989 issue of *AJR*.**

Received August 12, 1988; revision requested November 1, 1988; revision received November 25, 1988; accepted December 7, 1988.

This work was supported by National Institute of Neurological Diseases and Stroke grant 5-R01-NS19855 awarded to E. Courchesne.

[1] The Neuropsychology Research Laboratory, Children's Hospital Research Center, San Diego, CA 92123.

[2] Department of Radiology and Magnetic Resonance Institute, University of California, San Diego, School of Medicine, 225 Dickinson St., San Diego, CA 92103-1990. Address reprint requests to G. A. Press.

[3] Department of Pathology, University of California, San Diego, School of Medicine, San Diego, CA 92103-1990.

***AJNR* 10:659–665, July/August 1989**
0195–6108/89/1004–0659

received long TR examinations that were cardiac gated to every other or every third heartbeat. The pulse sequence parameters (2400–3800/20,70/2–4) yielded proton-density- and T2-weighted images, respectively. A presaturation RF pulse for eliminating blood-flow artifacts along the Z axis (flow void=1) was also used. Nongated long TR sequences performed on cadaver brains had the parameters, 1800–3000/20,70/4. Slices obtained in all sequences were separated by a 2.5-mm gap. A 28-sec T1-weighted scout sequence (200/20/1, 24-cm FOV, and 256 × 128 matrix) in the axial and sagittal plane was used to verify precise positioning of the subject or specimen brain prior to performing the protocol sequences.

Before MR, the specimen brains were fixed for 2–4 weeks in 10% neutral-buffered formalin. After MR, the cerebellum and brainstem were separated from the cerebral hemispheres and sectioned in the sagittal plane at a thickness of 5 mm. The tissue blocks were dehydrated in a graded series of alcohols, cleared in xylene, and embedded in paraffin. Sagittal microtome sections of the cerebellum and brainstem were cut at a thickness of 15 $\mu$m by using a Multirange Microtome.[†] Adjacent anatomic sections corresponding closely to the MR sections obtained by our protocol were stained with hematoxylin and eosin and Luxol fast blue–cresyl violet. The normal anatomic features of the cerebellar vermis and hemispheres visualized on MR and on the corresponding anatomic sections were determined by comparison with standard references of neuroanatomy [16, 17], myelin-stained cerebellar sections [18, 19], and cerebellar embryogenesis and development [20–23].

Many systems of nomenclature have been used to describe the normal anatomy of mammalian and human cerebellums [18, 21, 24]. In this report we follow closely the terminologies chosen by Ito [21] and Larsell [24].

## Results

### *Anatomic Features of the Vermis on a Sagittal Microtome Section*

The vermis represents the median segment of the cerebellum that is separated from each of the hemispheres by a shallow surface indentation, the paramedian sulcus. On a midline sagittal section (Fig. 1A), the ventral surface of the vermis is separated from the brainstem by three CSF-filled spaces that are oriented vertically [18, 25]. Superiorly, the precentral fissure separates the vermis from the inferior colliculi of the quadrigeminal plate. In the middle, the fourth ventricle separates the vermis from the dorsal surface of the pons and upper medulla. Inferiorly, the vallecula separates the vermis from the inferior medulla. Posteriorly, the cisterna magna separates the vermis from the meninges overlying the inner table of the occipital bone.

*Lobar and lobular divisions.*—The transverse-oriented primary and posterolateral fissures divide the vermis and cerebellar hemispheres into three major components: the anterior, posterior, and flocculonodular lobes [21] (Table 1). Two important nomenclatures are in common use for the designation of the lobules of the vermis. In one system, the vermis is divided into an anterior lobe containing three lobules (lingula, centralis, and culmen); a posterior lobe with five lobules (declive, folium vermis, tuber vermis, pyramis, and uvula); and one additional lobule, the nodulus or vermian portion of the flocculonodular lobe [21]. Although these names of the lobules continue to appear in the anatomic literature, another nomenclature widely used in physiologic studies of the cerebellum applies Roman numerals to 10 lobules in the vermis and lateral expansions in the hemispheres [24]. The two nomenclatures are listed in Table 1. In this report the Roman numeral designations are used only when necessary for clarity.

The lobules of the anterior vermis are bounded by the superior medullary velum anteriorly and the primary fissure posteriorly. The precentral fissure separates the lingula and centralis, while the preculminate fissure separates the centralis and culmen (Fig. 1A).

The lobules of the posterior vermis are bounded by the primary fissure (which separates them from the anterior lobe) and the posterolateral fissure (which separates them from the nodulus). Several fissures within the posterior vermis separate its five lobules from one another: the superior posterior fissure separates the declive and folium vermis, the horizontal fissure separates the folium vermis and tuber vermis, the prepyramidal fissure separates the tuber vermis and pyramis, and the secondary fissure separates the pyramis and uvula (Fig. 1A).

The nodulus is a separate lobe of the vermis that contains only one lobule. It represents the vermian portion of the flocculonodular lobe of the cerebellum and is bounded posteriorly by the posterolateral fissure and anteriorly by the vallecula (Fig. 1A).

*Sublobular and foliate divisions.*—Each lobule of the vermis can be subdivided into one or more sublobules, each containing a variable number of folia. The folium represents the basic structural unit of the cerebellum seen at gross examination and resolved by MR. Each folium is a thin, transverse-oriented fold of cerebellar parenchyma that contains a core of white matter covered by a mantle of gray matter. The unfolded surface of a single folium is a few millimeters wide. The human vermis contains approximately 260 of these structural units [21].

*Organization of the white matter.*—The white matter of the vermis appears to radiate into the lobules from a central confluence, known as the corpus medullare. The corpus medullare lies posterior to the fourth ventricle (Fig. 1A). Depending on the lobule in which they are located, the white-matter cores of the individual folia of the vermis may represent second-, third-, or even higher-order branches of the white matter emanating from the corpus medullare. To facilitate description, the white-matter tracts that originate from the corpus medullare may be grouped into two major divisions. The anterior division innervates the anterior lobe (lingula, centralis, and culmen) while the posterior division connects with the posterior lobe (declive, folium vermis, tuber vermis, pyramis, and uvula), as well as the nodulus.

Numerous anatomic variations have been described in the second-, third- and higher-order white-matter branches within the vermis (reviewed in [26]). To avoid confusion, we will emphasize only a description of the branching pattern of the *primary* white-matter tracts originating from the corpus medullare; this branching pattern was nearly constant in our series of specimen brains and normal volunteers.

[†] LKB, Stockholm, Sweden.

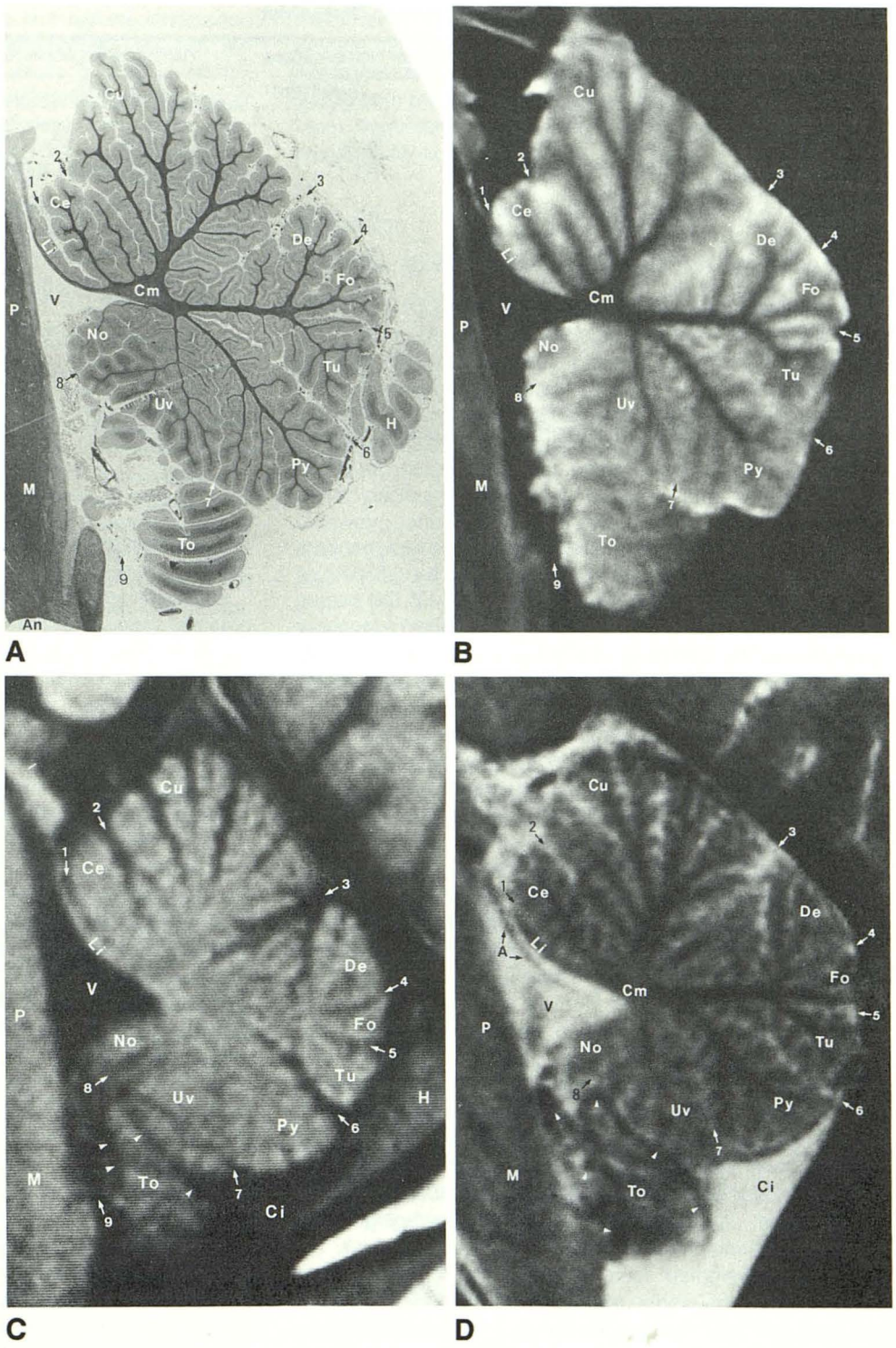


**Fig. 1.—Midsagittal sections through cerebellar vermis and brainstem. Sections through vermis must be thin (≤5 mm) to minimize volume averaging of adjacent cerebellar hemispheres (H) and tonsils (To).**

***A* and *B*, Microtome section of specimen brain (Luxol fast blue–cresyl violet myelin stain) (*A*) and corresponding proton-density-weighted 1.5-T MR image, 3000/20, before sectioning (*B*). White-matter branching within vermis is seen with remarkable fidelity on MR. Anterior division of white matter of corpus medullare (Cm) innervates lingula (Li), centralis (Ce), and culmen (Cu) of anterior lobe of vermis. Posterior division innervates declive (De), folium vermis (Fo), tuber vermis (Tu), pyramis (Py), and uvula (Uv) of posterior lobe as well as nodulus (No) of flocculonodular lobe of cerebellum. Fine secondary and tertiary white-matter branches to some regions (Uv) are shown well. An = anterior aspect of section; P = pons; M = medulla.**

***C* and *D*, T1-weighted, 600/20 (*C*), and cardiac-gated T2-weighted 3642/70 (*D*), images of 38-year-old male volunteer best show surface landmarks of vermis by accentuating signal-intensity difference between cerebellar parenchyma and CSF. Precentral cerebellar (1), preculminate (2), primary (3), superior posterior (4), horizontal (5), prepyramidal (6), secondary (7), and posterolateral (8) fissures around periphery of vermis are readily identified. Vallecula (9) separates vermis from inferior medulla (M), whereas cisterna magna (Ci) separates it from meninges overlying occipital bone. Curvilinear CSF flow artifact (A) may be identified within fourth ventricle (V) anterior to lingula on T2-weighted image. (Absence of curvilinear structure on T1-weighted image confirms its artifactual nature.) T2-weighted image also shows well pattern of white-matter branching within vermis (compare with *A* and *B*). Flow void within posterior inferior cerebellar arteries (*arrowheads*) is seen posterior to medulla in normal volunteer.**

1. Anterior division. In the most common arrangement, the lingula is situated along the ventral bank of the precentral fissure and receives a single primary tract from the corpus medullare. This single tract ascends adjacent to the dorsal aspect of the superior medullary velum. Each of our specimen brains (Fig. 1A) and normal volunteers demonstrated this anatomy. Others have reported that the lingula may include an additional segment between the ventral bank and the lobule centralis, "lingula duplex" [26], receiving an additional primary tract directly from the corpus medullare. This finding was not seen in our series.

The centralis receives one primary tract from the corpus medullare. The culmen also receives a single primary tract from which one or two secondary branches ascend into the

**TABLE 1: Components of the Human Cerebellum**

| Cerebellar Lobe | Vermian Lobule Nomenclature | | Hemispheric Lobule Nomenclature | |
|---|---|---|---|---|
| | Ito [21] | Larsell [24] | Ito [21] | Larsell [24] |
| Anterior | Lingula | I | – | HI[a] |
| | Centralis | II, III | Central lobule | HII, HIII |
| | Culmen | IV, V | Quadrangular lobule, anterior portion | HIV, HV |
| Posterior | Declive | VI | Quadrangular lobule, posterior portion | HVI |
| | Folium vermis | Superior VIIA | Semilunar lobule, superior portion | HVIIA |
| | Tuber vermis | Inferior VIIA | Semilunar lobule, inferior portion | HVIIA |
| | | VIIB | Gracile lobule | HVIIB |
| | Pyramis | VIIIA, VIIIB | Biventer | HVIII |
| | Uvula | IX | Tonsil | HIX |
| Flocculonodular | Nodulus | X | Flocculus | HX |

[a] Hemispheric counterpart of vermian lobule I is usually absent in humans [21].

anterior portion of the lobule (lobule IV), and three secondary branches supply the posterior portion of the lobule (lobule V).

2. Posterior division. A single primary tract of the corpus medullare gives rise to several (usually two to four) secondary branches to the declive (lobule VI) and a single secondary branch each to the folium and tuber vermis (combined lobules VIIA and VIIB) (Fig. 1A).

The major white-matter bundle supplying the pyramis may arise either as a primary tract directly from the corpus medullare (Fig. 1A) or as a large secondary branch of the primary tract that innervates also the declive and folium and tuber vermis [26].

Single primary white-matter tracts innervate the uvula and the nodulus along the inferior and anteroinferior surfaces of the vermis. The primary tract to the uvula subsequently splits into two secondary branches, which supply the entire lobule (Fig. 1A).

### *Overview of MR Imaging of the Vermis*

Early in our experience we noted that skull-surface landmarks were unreliable for positioning subjects and anatomic specimens for true sagittal images of the vermis. The small (6- to 12-mm) lateral dimension of the vermis, and its shorter anteroposterior dimension relative to that of the cerebellar hemispheres, can easily result in volume averaging of the hemispheres with the vermis if a tilt of the head remains. We obtained T1-weighted scout images in both the axial and sagittal planes to verify adequate head positioning in all subjects and anatomic specimens. The subsequent acquisition of thin (5-mm) sagittal sections using the protocol sequences provided optimal visualization of the vermis on the midline image.

Spin-echo pulse sequences that maximized the contrast between parenchyma and CSF showed the surface sulci and fissures of the cerebellum to best advantage. T1-weighted images (CSF much lower in signal intensity than parenchyma, Fig. 1C) or T2-weighted images (CSF much higher in signal intensity than parenchyma, Fig. 1D) were ideal for demonstrating the surface features of the cerebellum in vivo.

Excellent contrast between white and gray matter was obtained with proton-density-weighted (Fig. 1B) and T2-weighted (Fig. 1D) pulse sequences. Such images showed best the deeper anatomy of the vermis including the primary white-matter fiber tracts radiating from the corpus medullare to the individual lobules of the cerebellum. CSF in vivo, or fluid in the subarachnoid space in the postmortem state, was nearly isointense relative to the cortex on proton-density-weighted images, however, thereby obscuring the surface features (sulci and fissures) of the cerebellum.

Superior image quality on the long TR sequence required cardiac gating (every second or every third heartbeat) and a presaturation RF pulse (flow void-1) to further decrease artifacts due to CSF motion in the prepontine cistern and blood flow in the basilar artery and transverse and sigmoid sinuses. Images of eight to 10 5-mm-thick slices could be acquired in a single acquisition (scanning time, 30 or 60 min) using two or four excitations. A 2.5-mm interslice gap was chosen so that the entire cerebellum could be surveyed in the axial or coronal plane, whereas approximately 50% could be examined in the sagittal plane during a single acquisition.

### *Anatomic Features of the Vermis on Sagittal MR Sections*

*Surface features.*—The cerebellar vermis lies in the midline posterior to the brainstem. The quadrigeminal plate cistern merges inferiorly with the precentral fissure separating the vermis from the midbrain and superior medullary velum (Figs. 1C and 1D). The superior and inferior medullary vela meet at a sharp point called the fastigium to form the roof of the triangular fourth ventricle, which lies between the vermis and the pons. The inferior medullary velum is diaphanous and typically is not resolved on 5-mm-thick images.

Because the great fissures and smaller sulci of the vermis are oriented perpendicular to the midline, sagittal T1-weighted (Fig. 1C) and T2-weighted (Fig. 1D) images display most

accurately the depth of these important surface landmarks. The preculminate, prepyramidal, and primary fissures are relatively wide and may be seen easily on MR in normal volunteers. The horizontal and secondary fissures are thinner and more difficult to resolve. Nevertheless, they can be identified confidently in most subjects on T1- and T2-weighted images. The CSF spaces lying between the individual folia of the vermis are shallow and thin. Generally speaking, they can be resolved over the centralis, culmen, declive, folium vermis, tuber vermis, and pyramis, but may be obscured over the lingula, uvula, and nodulus. They are often best seen on T2-weighted images (Fig. 1D).

The cerebellar tonsils have an intimate relationship with the vermis [27]. The tonsils are bilateral, oval-shaped masses of tissue that lie close to the midline. Along their lateral margins they attach to the inferomedial aspects of the cerebellar hemispheres. The other surfaces of each tonsil abut on fissures and cisterns that separate them from the cerebullum, vermis, and brainstem. Several inferior vermian lobules (nodulus, uvula, and pyramis) are indented to a variable degree by the superior aspects of the tonsils in normal subjects. Moreover, the inferior portions of the tonsils lie within the cisterna magna, and may touch each other in the midline immediately caudal to the vermis. For these reasons, the tonsils can be difficult to distinguish from the nodulus, uvula, and pyramis on midline sagittal images. Helpful clues to identifying a tonsil include its defined ovoid contour, the orientation of its axis parallel to the posterior surface of the medulla, its more sharply convex lower border with greater caudal extent, and the position of the choroid plexus and supratonsillar segment of the posterior inferior cerebellar artery atop the apex of the ovoid [25].

*Deep features.*—On proton-density-weighted (Fig. 1B) and T2-weighted (Fig. 1D) images, the gray matter overlying the folia of the vermis forms a bright band that is thicker where the surfaces of two lobules are immediately adjacent in the depths of the fissures. The sparse and relatively dark white matter located centrally appears to project radially into the anterior and posterior lobes of the vermis from a small zone just posterior to the fastigium. Sagittal sections through the paramidline hemispheres can be distinguished from those through the vermis due to the greater abundance of white matter, which forms a much larger central body within the hemispheres [27]. Moreover, the gray and white matter of the tonsils, arranged in a regular "hatch-mark" fashion at a 45-90° angle to the posterior surface of the medulla [25], can also be distinguished from the radial arrangement of the vermian white-matter bundles [27].

Each of the six or seven primary tracts that constitute the anterior and posterior divisions of the vermian white matter can be distinguished on proton-density-weighted or T2-weighted (Fig. 1D) images in vivo. Secondary branches innervating lobules IV and V of the culmen, the declive, and the folium and tuber vermis are also readily detected. In some instances, the tonsils indent the inferior vermis sufficiently to obscure independent visualization of the two secondary white-matter branches within the uvula.

Visualization of the individual white-matter cores distinct from overlying gray matter of each *folium* of the vermis seems beyond the capability of our in vivo MR protocol at present. Nevertheless, proton-density- and T2-weighted images acquired with the specimen brain protocol (four excitations per slice) frequently can resolve many of these most slender white-matter bundles (Fig. 1B).

## Discussion

### *Functional Anatomy and Connections of the Vermis*

Somatic motor (midline musculature) and vestibuloocular activities are regulated and coordinated by the vermian cortex [21, 28]. Cortical (Purkinje) neurons project to the fastigial nuclei, which in turn project to reticular and vestibular neurons of the brainstem. Subsequent ascending pathways controlled by Purkinje cells within the declive, folium, and tuber influence brainstem nuclei governing ocular movements (e.g., oculomotor nucleus); descending (reticulo- and vestibulospinal) pathways controlled by other regions of vermian cortex reach anterior horn cells of the spinal cord. Cortex of the vermis also influences neural pathways concerned with level of attention [16, 28], sensory function [29], corticoneostriatal interactions (Ryan LJ, personal communication), autonomic activities [30], motivation [31, 32], memory [33, 34], and behavior [31, 32, 35].

Such functional diversity is reflected in regional specialization of the vermis [28]. For instance, the anterior lobe receives mainly spinal input (from spino- and cuneocerebellar fibers) and relatively little cerebral cortical input. Efferent fibers from the anterior lobe are sent primarily to lower brainstem systems. The posterior lobe receives major input from cerebral cortex (motor, somatosensory, visual, auditory, and association areas), tectum, and hippocampus, but sparse spinal input. Efferents from the posterior lobe connect with the midbrain, thalamus, and hypothalamus, as well as lower brainstem systems [28]. Specialization is epitomized by the declive, folium, and tuber—the auditory and visual areas of the vermis—which are critical for establishing certain types of long-term memory traces [34].

Lesions of the vermis generally result in disorders of eye movements (e.g., horizontal nystagmus), abnormal posture of the head, disturbances of stance and gait, dysmetria, succession deficits, and kinetic tremor [28]. Impairments in memory and consciousness, dysarthria, and past-pointing occur less often [28].

### *Development Variants*

Hypoplasia (undergrowth) and partial or complete agenesis (nongrowth) of the vermis have been reported [36–38]. Although most cases are sporadic, familial agenesis may occur [38]. In all instances of partial agenesis, the anterosuperior portion of the vermis is preserved, presumably because fusion of the vermis proceeds from rostral to caudal during the second month of gestation [27].

The clinical picture of patients with partial or complete agenesis of the vermis is neither uniform nor characteristic

[36]. Although inability to walk, nystagmus, head- and body-turning attacks, and mental retardation are associated frequently with partial vermian agenesis, a minority of patients may be completely asymptomatic [36, 38, 39]. In one sibship, agenesis of the vermis varied from partial to complete; all four patients had mental retardation and developmental delay. Additional abnormalities included hypotonia, episodic hyperpnea, lack of interest in the environment, involuntary facial movements, and abnormal speech and language development [38]. Occasionally, however, psychomotor retardation and neurologic deficits may be absent, even in patients with complete agenesis [36, 38]. Agenesis of the vermis may be accompanied by few or no other CNS abnormalities, or by a spectrum of malformations involving the cerebellar hemispheres and dentate nucleus (e.g., hypoplasia and gray-matter heterotopias) or supratentorial structures (e.g., callosal hypoplasia or agenesis) [36–38]. Symptoms, when present in these patients, may relate to the extravermian locus of abnormality [36, 38].

Hypoplasia of the vermis may be regionally localized (e.g., superoposterior vermis in autism) [40, 41] or diffuse (e.g., Down syndrome) [42]. There are no reports of hypoplasia involving only anterosuperior vermian regions. In all reported cases, vermian hypoplasia is accompanied also by hypoplasia of the cerebellar hemispheres [40, 41, 43, 44].

### *Atrophic Conditions*

After normal development, the vermis may be affected by metabolic or degenerative disorders associated with parenchymal atrophy [45]. In contrast to the developmental anomalies described above, which spare the anterosuperior lobules of the vermis, several common atrophic conditions involve predominantly this portion of vermian cortex. For instance, selective atrophy, most marked in the cortex of the anterior and superior lobules of the vermis and in the paramedian portions of the anterior lobes of the hemispheres, is frequently found in chronic alcoholics [45]. The cortical atrophy is evidenced by wide, deep sulci and thinned folia. Strikingly similar clinical and pathologic findings are demonstrated also in parenchymatous cerebellar atrophy of Holmes, a relatively common degenerative disorder of the cerebellar system [45]. Other degenerative disorders of the cerebellum involve the cerebellar hemispheres to a greater degree than the vermis (e.g., olivopontocerebellar atrophy).

## Conclusions

Improvements in MR technology permit the display of many important features of the cerebellar vermis not previously shown. Learning the detailed normal sagittal anatomy of the vermis has helped us to recognize and differentiate the pathologic alterations known to accompany malformations (e.g., hypoplasia and agenesis); genetic (e.g., Down syndrome) and idiopathic (e.g., autism) disorders; metabolic diseases (e.g., alcoholism); and system degenerations (e.g., parenchymatous cerebellar atrophy). Clinical symptomatology may vary depending on the lobules within the vermis that are affected as well as the time and type of insult. Heretofore, it has not been possible to link with precision active neurologic signs, symptoms, and type of insult to lesion status and extent in vivo. The present MR report opens up this possibility.

## REFERENCES


1. Han JS, Bonstelle CT, Kaufman B, et al. Magnetic resonance imaging in the evaluation of the brainstem. *Radiology* **1984**;150:705–712
2. Bradley WG Jr, Waluch V, Yadley RA, Wycoff RR. Comparison of CT and MR in 400 patients with suspected disease of the brain and cervical spinal cord. *Radiology* **1984**;152:695–702
3. Randell CP, Collins AG, Young IR, et al. Nuclear magnetic resonance imaging of posterior fossa tumors. *AJR* **1983**;141:489–496
4. Lee BCP, Kneeland JB, Deck MDF, Cahill PT. Posterior fossa lesions: magnetic resonance imaging. *Radiology* **1984**;153:137–143
5. New PFJ, Bachow TB, Wismar GL, Rosen BR, Brady TJ. MR imaging of the acoustic nerves and small acoustic neuromas at 0.6 T: prospective study. *AJNR* **1985**;6:165–170
6. Daniels DL, Millen SJ, Meyer GA, et al. MR detection of tumor in the internal auditory canal. *AJNR* **1987**;8:249–252
7. Gentry LR, Jacoby CG, Turski PA, et al. Cerebellopontine angle-petromastoid mass lesions: comparative study of diagnosis with MR imaging and CT. *Radiology* **1987**;162:513–520
8. Enzmann DR, O'Donohue J. Optimizing MR imaging for detecting small tumors in the cerebellopontine angle and internal auditory canal. *AJNR* **1987**;8:99–106
9. Press GA, Hesselink JR. MR imaging of cerebellopontine angle and internal auditory canal lesions at 1.5 T. *AJNR* **1988**;9:241–251
10. Spinos E, Laster DW, Moody MD, Ball MR, Witcofski RL, Kelly DL Jr. MR evaluation of Chiari I malformations at 0.15 T. *AJNR* **1985**;6:203–208
11. Lee BCP, Deck MDF, Kneeland JB, Cahill PT. MR imaging of the craniocervical junction. *AJNR* **1985**;6:209–213
12. Barkovich AJ, Wippold FJ, Sherman JL, Citrin CM. Significance of cerebellar tonsillar position on MR. *AJNR* **1986**;7:795–799
13. Wolpert SM, Anderson M, Scott RM, Kwan ESK, Runge VM. Chiari II malformation: MR imaging evaluation. *AJNR* **1987**;8:783–792
14. Naidich TP, Zimmerman RA. Common congenital malformations of the brain. In: Brant-Zawadzki M, Norman D, eds. *Magnetic resonance imaging of the central nervous system.* New York: Raven, **1987**:131–150
15. van der Knaap MS, Valk J. Classification of congenital abnormalities of the CNS. *AJNR* **1988**;9:315–326
16. Nieuwenhuys R, Voogd J, Huijzen C. *The human central nervous system: a synopsis and atlas*, 2nd ed. New York: Springer-Verlag, **1981**
17. Carpenter MB. *Human neuroanatomy*, 7th ed. Baltimore: Williams & Wilkins, **1976**
18. Angevine JB Jr, Mancall EL, Yakovlev PI. *The human cerebellum. An atlas of gross topography in serial sections.* Boston: Little, Brown, **1961**
19. DeArmond SJ, Fusco MM, Dewey MM. *Structure of the human brain: a photographic atlas.* New York: Oxford University, **1976**
20. Fox CA, Snider RS, eds. *The cerebellum.* Amsterdam: Elsevier, **1967**
21. Ito M. *The cerebellum and neural control.* New York: Raven, **1984**
22. Lemire RJ, Loeser JD, Leech RW, Alvord EC Jr. *Normal and abnormal development of the human nervous system.* Hagerstown, MD: Harper & Row, **1975**
23. Larsell, O. The development of the cerebellum in man in relation to its comparative anatomy. *J Comp Neurol* **1947**;87:85–129
24. Larsell O. The cerebellum. A review and interpretation. *Arch Neurol Psychiatry* **1937**;38:580–607
25. Yousefzadeh DK, Naidich TP. US anatomy of the posterior fossa in children: correlation with brain sections. *Radiology* **1985**;156:353–361
26. Larsell O, Jansen J. *The comparative anatomy and histology of the cerebellum,* vol. 3. *The human cerebellum, cerebellar connections and cerebellar cortex.* Minneapolis: University of Minnesota, **1972**
27. Press GA, Murakami J, Courchesne E, et al. The cerebellum in sagittal plane—anatomic-MR correlation: 2. The cerebellar hemispheres. *AJNR* **1989**;10:667–676
28. Gilman S, Bloedel J, Lechtenberg R. *Disorders of the cerebellum.* Philadelphia: Davis, **1981**

29. Crispino L, Bullock TH. Cerebellum mediates modality-specific modulation of sensory responses of midbrain and forebrain in rat. *Proc. Natl. Acad. Sci USA* **1984**;81:2917–2920
30. Haines DE, Dietrichs E. On the organization of interconnections between the cerebellum and hypothalamus. In: King JS, ed. *New concepts in cerebellar neurobiology*, vol. 12. New York: Liss, **1987**:113–149
31. Supple WF, Leaton AN, Fanselow MS. Effects of cerebellar vermal lesions on species-specific fear responses, neophobia, and taste-aversion learning in rats. *Physiol Behav* **1987**;39:579–586
32. Ball G, Micco DJ Jr, Berntson G. Cerebellar stimulation in the rat: complex stimulation-bound oral behaviors and self-stimulation. *Physiol Behav* **1974**;13:123–127
33. Newman PP, Reza H. Functional relationships between the hippocampus and the cerebellum: an electrophysiological study of the cat. *J. Physiol* (Lond) **1979**;287:405–426
34. Leaton RN, Supple WF. Cerebellar vermis: essential for long-term habituation of the acoustic startle response. *Science* **1986**;232:513–515
35. Reis DJ, Doba N, Nathan MA. Predatory attack, grooming, and consummatory behaviors evoked by electrical stimulation of cat cerebellar nuclei. *Science* **1973**;182:845–847
36. Macchi G, Bentivoglio M. Agenesis or hypoplasia of cerebellar structures. In: Vinken PJ, Bruyn GW, eds. *Congenital malformations of the brain and skull.* Amsterdam: North-Holland, **1977**:367–393
37. Mercuri S, Curatolo P, Giuffre R, DiLorenzo N. Agenesis of the vermis cerebelli and malformations of the posterior fossa in childhood and adolescence. *Neurochirurgia* (Stuttg) **1979**;22:180–188
38. Joubert M, Eisenring JJ, Robb JP, Andermann F. Familial agenesis of the cerebellar vermis. *Neurology* **1969**;19:813–825
39. DeMorsier G, Laville F. Etudes sur les dysraphies cranio-encephaliques. VIII. Dysraphies du diencephale de la loge hypophysaire, du telencephale inferieur et du cervelet. *Acta Neurol Belg* **1962**;23:443–453
40. Courchesne E, Hesselink JR, Jernigan TL, Yeung-Courchesne R. Abnormal neuroanatomy in a nonretarded person with autism: unusual findings with magnetic resonance imaging. *Arch Neurol* **1987**;44:335–341
41. Courchesne E, Yeung-Courchesne R, Press GA, Hesselink JR, Jernigan TL. Hypoplasia of cerebellar vermal lobules VI and VII in infantile autism. *N Engl J Med* **1988**;318:1349–1354
42. Benda CE. *Down's syndrome. Mongolism and its management.* New York: Grune & Stratton, **1969**:134–166
43. Jervis GA. Early familial cerebellar degeneration (report of three cases in one family). *J Nerv Ment Dis* **1950**;111:398–407
44. Sarnet HB, Alcala H. Human cerebellar hypoplasia. *Arch Neurol* **1980**;37:300–305
45. Adams JH, Corsellis JAN, Duchen LW, eds. *Greenfield's neuropathology*, 4th ed. New York: Wiley, **1985**